Journal of Applied Electrochemistry **32**: 1269–1278, 2002.

Cementation and corrosion at a RDE: Changes in flow and transfer phenomena induced by surface roughness

C. ALEMANY[1], M. AUROUSSEAU[1,*], F. LAPICQUE[2] and P. OZIL[1]
[1]*Laboratoire d'Electrochimie et de Physicochimie des Matériaux et des Interfaces, UMR 5631 CNRS-INPG-UJF, ENSEEG, BP 75, F-38402 St Martin d'Hères, France*
[2]*Laboratoire des Sciences du Génie Chimique, CNRS-ENSIC, BP 451, F-54001 Nancy, France*
*(*author for correspondence, e-mail: marc.aurousseau@efpg.inpg.fr)*

Received 5 November 2001; accepted in revised form 30 July 2002

Key words: cementation, corrosion rate, rotating disc electrode, surface roughness

Abstract

Cementation and corrosion were investigated in a batch cell to highlight the improvement of the kinetics observed after a certain lapse of time. Experiments on cementation with the Cd(II)/Zn and Ag(I)/Cu systems, and on corrosion with the Ce(IV)/Zn and Cr(VI)/Zn couples, were carried out on a rotating disc electrode immersed in relatively concentrated solutions. Time variations of the concentration of the reacting species and SEM observations showed that the change in reaction kinetics was due to the roughness of the changing surface of the electrode, depending on the chemical system considered. For corrosion, the average roughness was shown to exceed the thickness of the Nernst diffusion layer, and the rougher surface created allows local flow disruption and mass transfer enhancement. Besides, corrosion by Cr(VI) species results in greater roughness of the metal surface with more significant flow disruption than with Ce(IV) at the same concentration.

List of symbols

A	geometrical electrode area (m^2)
C	concentration of electroactive species (mol m^{-3})
C_0	initial concentration of electroactive species (mol m^{-3})
D	diffusion coefficient (m^2 s^{-1})
E_{cem}	cementation potential (V)
F	faradaic constant (C mol^{-1})
F	function defined in [42] for expression of v_z
f	function defined by Relation 3
i	current density (A m^{-2})
i_{lim}	limiting current density (A m^{-2})
K	overall rate constant (s^{-1})
K_{thermo}	equilibrium constant of reaction
k	mass transfer coefficient (m s^{-1})
k_s	surface roughness from [35] used in Relation 5 (m)
l_c	average thickness of the layer of dissolved metal at t_c (m)
m_c	specific mass of deposited or dissolved metal at t_c (kg m^{-2})
n	number of electrons involved
r	radius of the disc electrode (m)
r_c	depth of cavity at critical time t_c (m)
Re	Reynolds number: $\omega r^2/v$
Re_{surf}	Reynolds number close to the irregular surface defined by Relation 10
Re_t	transition Reynolds number from [35] and defined by Relation 5
Sc	Schmidt number, v/D
Sh	Sherwood number, $k\,r/D$
Sh_{surf}	Sherwood number close to the irregular surface defined by Relation 10
t	time (s)
t_c	critical or transition time (s)
T	temperature (°C)
V	volume of solution (m^3)
V_0	volume of solution at $t = 0$ (m^3)
v_z	radial velocity of the fluid at distance z (m s^{-1})
v_{rc}	radial component of velocity at distance r_c from the disc (m s^{-1})
X	conversion extent
z	distance from the disc plan (m)

Greek symbols

δ	thickness of the diffusion layer (m)
v	kinematic viscosity (m^2 s^{-1})
ζ	dimensionless coordinate $= z(\omega/v)^{1/2}$
ω	rotation rate of the RDE (rad s^{-1})

Subscripts

0	initial
1	first period of the cementation or corrosion run
2	second period of the run

c critical or transition
j number of sample drawn
Levich related to Levich's equation from Relation 4
mod modified for mass transfer coefficient by Relation 6

1. Introduction

Cementation is an electrochemical process used in industry for the removal of metal ions from dilute solutions either for liquid purification or metal recovery. Its main domains of application are hydrometallurgy [1–4], electroplating [5, 6], electrowinning [7, 8], and waste treatment [9–11]. Its consists in reducing a noble or toxic metal ion M^{m+} by using a more electropositive sacrificial metal S according to the general heterogeneous reaction:

$$sM^{m+} + mS \rightleftharpoons sM + mS^{s+} \quad (1)$$

Although the process has been used in practice for a long time because of easy, low cost implementation, the elementary processes have not yet been fully elucidated. In particular, the exact influence on cementation kinetics of the surface evolution resulting from simultaneous cathodic deposition and anodic dissolution is still under discussion.

Cementation reactions are generally characterised by a large negative difference in free enthalpy, corresponding to equilibrium constants K_{thermo} greater than 10^{10}. Moreover, for most systems [12–14], the reaction rate is controlled by mass transfer of the noble metal ion, and the kinetics of cementation is described by an overall first-order reaction rate. Therefore, the logarithm of M^{m+} concentration, C, is expected to vary linearly with time, for the case of a batch reactor with uniform composition, as follows:

$$\ln\left(\frac{C_0}{C}\right) = Kt = k\frac{A}{V}t \quad (2)$$

if K is the overall rate constant, k the liquid–solid mass transfer coefficient, V the volume solution and A is approximated by the geometrical area of the electrode. However, for most M/S couples, a change in the slope expected from the above variation is observed for conversions of M^{n+} ranging from 5 to 20%, and the kinetics of the second period is enhanced by a factor up to 8 [15–17]. The transition in kinetics is usually accompanied by a change in the deposit morphology [18]. This rate enhancement may be caused by increases in the reacting electrode area, due to surface modification, and in mass transfer due to turbulence phenomena at the rougher surface. The conclusions drawn by the published investigations differ from each another, possibly because of the different techniques used and the different systems considered. It has often been suggested (e.g., in [16]) that the change in kinetics corresponded to a critical specific weight m_c causing modifications of flow phenomena and mass transfer rates. However, from the published data, m_c appears to be affected by the initial concentration of the noble metal [19] and the nature of the M/S system. The rate enhancement could be observed even at initial concentrations of the reacting ion below 0.2 mol m^{-3}, for weight deposits of the order of 10^{-3} kg m^{-2}, corresponding to average thickness far below 1 μm: in this case, the occurrence of turbulence flow induced by the surface roughness seems unlikely [20, 21]. Impedance spectroscopy has been used for assessment of the change in active area: no significant change was observed at the transition point for the example of the $AgNO_3$/Cu displacement at low concentrations [22], but electrode blockage could be put into evidence by impedance measurements, either at the early stages of the operation from a nitrate medium [23], or later from the cyanide bath also used in [22]. The models relying upon the critical deposit weight appears insufficient for complete interpretation of the transition. Other concepts, for example, surface activation and morphology index, have been suggested in an attempt to model the transition of regime [24].

The present paper was focused at a better understanding of the enhancement of the kinetics in relation to the morphology of the metal deposited or corroded. Solutions of appreciable concentration were used, resulting in specific weights of metal m_c of the order of 0.5 kg m^{-2}, corresponding to an average thickness/roughness above 10 μm. Both cementation and corrosion reactions were investigated in order to quantify the kinetics change in terms of mass transfer rates and to observe the effect of the surface roughness induced by deposition or dissolution. The RDE configuration was selected because of its well-controlled flow and transfer phenomena, at least for smooth surfaces of the disc. Cementation was studied with Ag(I)/Cu and Cd(II)/Zn systems whereas Ce(IV)/Zn and Cr(VI)/Zn couples were used for corrosion experiments.

2. Experimental details

All chemical products were of analytical grade (Normapur, Prolabo, France). The initial concentration of reacting species ranged from 4.4 to 10 mol m^{-3} depending on the reaction investigated. The ionic strength of all solutions was adjusted at 1.0 M by addition of sodium nitrate or sodium sulfate, depending on the system used (Table 1): migration phenomena and local variations of the ionic strength could then be neglected. Moreover the pH of the solutions reported in Table 1 were chosen to prevent the formation of insoluble hydroxides or complexes, using Pourbaix diagrams [25] and pH-concentration diagrams. Finally, the side corrosion due to the action of acidic solutions was shown to be negligible throughout the experiments, by considerations of mass balances and reaction stoichiometry. The amount of metal dissolved by H^+ represents less than 0.1% of the amount of S^{s+} formed in regular cementation, that is, in the presence of M^{m+} species.

Table 1. Equilibrium thermodynamic constant K_{thermo} and experimental diffusion coefficient D at 25 °C and 1.0 M ionic strength for the systems under study

System	pH	Soluble form	K_{thermo}	$D/m^2\ s^{-1}$ (this study)	$D/m^2\ s^{-1}$ (literature data)
Ag(I)/Cu/NO_3^-	2.5	Ag^+	$10^{15.5}$	1.9×10^{-9}	1.7×10^{-9} [26]
Cd(II)/Zn/SO_4^{2-}	6	$Cd(SO_4)_4^{6-}$	$10^{12.2}$	7.0×10^{-10}	6.6×10^{-10} [27]
Ce(IV)/Zn/SO_4^{2-}	1.5	$Ce(SO_4)_3^{2-}$	$10^{80.3}$	3.5×10^{-10}	3.7×10^{-10} [28]
Cr(VI)/Zn/SO_4^{2-}	1.5	$Cr_2O_7^{2-}$	∞	7.7×10^{-10}	8.9×10^{-10} [29]

Cementation and corrosion experiments were carried out using a RDE Tacussel EDI 101T device. Electrodes of diameter 5 and 9 mm were machined out of high purity copper or zinc (>99.9%) and embedded into PTFE rods of 11 and 16 mm, respectively. The metal surface was carefully polished with diamond pastes with decreasing particle size to 1 μm. The electrodes were immersed in double-walled glass vessels. Depending on the electrode diameter, the solution volume introduced, V_0, was fixed at 100 and 325 cm^3 so that the specific area of the electrode A/V_0 appearing in Relation 3, was kept constant at 0.196 m^{-1} for the two configurations. The temperature T was fixed at 25 °C for all runs. The electrolyte solutions were purged by bubbling ultrapure nitrogen for 30 min, and then blanketed during the experiments. One cm^3 fractions of liquid were sampled at regular intervals for analysis by atomic absorption using a Varian AA-10 spectrophotometer. The time variations of the concentrations were corrected for the progressive decrease of the solution volume and Relation 2 was then modified into:

$$\sum_{1}^{j} \frac{V_{j-1}}{V_0} \ln\left(\frac{C_{j-1}}{C_j}\right) = \frac{kA}{V_0} t_j \qquad (3)$$

where running subscript j corresponds to the number of samples drawn at time t_j. For convenience, the expression for the time variations of concentrations in the left-hand part of Relation 3 was denoted $f(C_0/C)$ in the Figures.

The surfaces of metal deposited or corroded were observed and analysed by using a 6400 Jeol coupling scanning electron microscopy (SEM) and energy dispersive spectroscopy (EDS). Corroded surfaces were also observed by optical microscopy using a Leica DMRM instrument.

3. Results

3.1. *Preliminary considerations and experiments*

For the reactions under study, the equilibrium constants K_{thermo} calculated at 25 °C from the standard half-cell potentials [25], are greater than 10^{12} (Table 1), corresponding to irreversible reductions of the reacting species.

The cementation reaction can be considered as a deposition process at the cathode coupled to a dissolution process at the anode. The limiting step can thus be determined independently by using techniques such as Evans diagrams for corrosion reactions. Evans diagrams are obtained by superimposing the anodic polarisation curve on the cathodic one, recorded separately at the same rotation speed. For the present study, the cathodic processes were the reduction of Ag(I) or Cd(II) species on a Ag or Cd surface, respectively, or the reduction of Ce(IV) or Cr(VI) on a gold surface. The anodic reactions were zinc or copper dissolution. The potential scanning rate was 10 mV s^{-1} to avoid significant changes to the electrode surface, while ensuring quasi-steady state voltammetric behaviour. The operating cementation point was obtained for identical absolute values of the current density for reduction and oxidation, assuming identical anodic and cathodic area on the disc for cementation experiments. The cementation point of coordinates (E_{cem}, $i = 0$) was found for all cases to be located on the diffusion plateau of the reduction wave, corresponding to mass transfer-controlled operation, as exemplified in Figure 1 for the example of Cd(II)/Zn couple. The technique was validated by the low deviation (below 3%) observed on E_{cem} values determined either from Evans' diagrams or by measuring the potential in the first instants of the reaction.

The diffusion coefficient D of the cementing species was determined from the limiting current density of the reduction, i_{lim}, on the RDE surface and using Levich's relation:

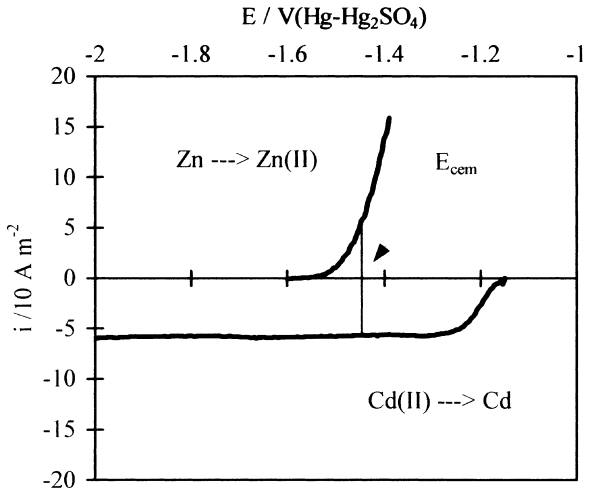

Fig. 1. Example of Evans' diagram for Cd(II)/Zn system with 4.45 mol m^{-3} Cd(II) species; $\omega = 157$ rad s^{-1} and $T = 25$ °C.

$$i_{\lim} = -0.62D^{2/3}v^{-1/6}\omega^{1/2}nFC \quad (4)$$

The kinematic viscosity, v, was measured by Ubbelohde technique at 0.99×10^{-6} m^2 s^{-1} for all the solutions used. The D values obtained and reported in Table 1 are in good agreement with published data for comparable electrolyte solutions [26–29], respectively (deviations around 6%, greater values resulting from non identical support electrolyte).

3.2. *Cementation*

3.2.1. *Kinetic curves and role of the formed deposit*

The cementation runs revealed the existence of two periods, with a well-marked transition point and a higher reaction rate for the second period (Figures 2 and 3). For the case of Cd(II)/Zn system, detachment of deposit was induced by tapping the rotating device at regular lapses of time. These times corresponded to conversion extents of the cementing species being 1, 2 and 3 times the conversion extent $X_{\mathrm{Cd(II)},c}$ obtained at the transition – or critical – point in 'normal' conditions, that is, without hitting the disc system. This artificial means allowed the reaction rate to be kept constant at its level during the first period (Figure 2). The kinetic enhancement was observed again with an intensity comparable to that in 'normal' conditions, after 177 min in the example given in this Figure. This time lapse is approximately equal to the time required for a conversion extent fourfold the critical conversion $X_{\mathrm{Cd(II)},c}$, at 170 min. As a matter of fact, the part of curve (b) after the third deposit fall can be deduced from curve (a) by translation in time and in $f(C_0/C)$.

Deposited silver is less compact, with a lower adherence, which resulted in its natural fall from the disc. The

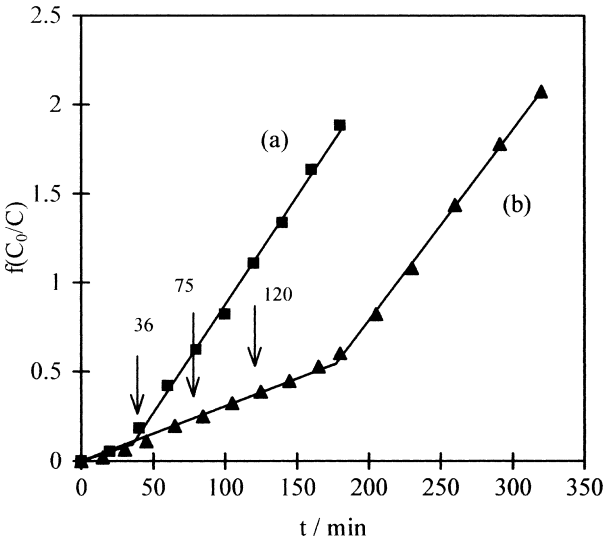

Fig. 2. Kinetic curves for the Cd(II)/Zn system in a sulfate medium with $\omega = 157$ rad s^{-1}, $C_0 = 4.45$ mol m^{-3}, $A = 0.196$ cm^2, $V_0 = 100$ cm^3; (a) continuous run and (b) run with forced falls of Cd deposit indicated by arrows and corresponding times.

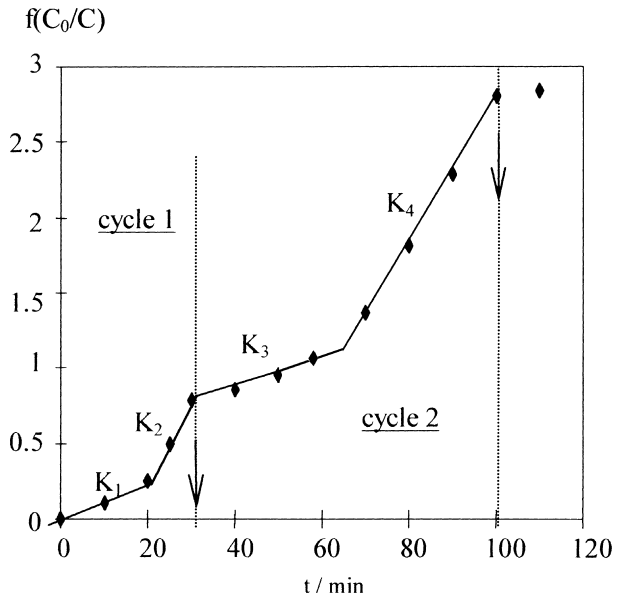

Fig. 3. Kinetic curves for the Ag(I)/Cu system in a nitrate medium with spontaneous falls of Ag deposit, indicated by arrows; $\omega = 157$ rad s^{-1}, $C_0 = 10$ mol m^{-3}, $A = 0.196$ cm^2, $V_0 = 100$ cm^3.

fall induced a sudden decrease in the reaction rate, back to that observed for the first period of the run, as shown in Figure 3 with the Ag(I)/Cu couple. The first fall occurred after 32 min, while the second was observed after 100 min as in Figure 3, due to the consumption of the Ag(I) species in the solution. The cementation consists of two cycles separated by the fall of deposited metal, and the periodic process 'growth-fall' appears perfectly repeatable, $K_1 = 1.9 \times 10^{-4}$ s^{-1} with $K_3 = 1.8 \times 10^{-4}$ s^{-1} and $K_2 = 8.4 \times 10^{-4}$ s^{-1} with $K_4 = 7.7 \times 10^{-4}$ s^{-1}, taking into account the experimental error on K determination, estimated by replicate experiments at 8%. This clearly shows the role of the formed deposit on the rate constant K and therefore on the mass transfer coefficient k (Relations 2 and 3).

Moreover, for the case of silver, the critical mass of deposit decreased from 1.20 kg m^{-2} for the first cycle to 0.79 kg m^{-2} for the second. In addition the duration of one period increased along the run, passing from 20 to 33 min for the first period (constants K_1 and K_3), and from 12 to 35 min for the second period (constants K_2 and K_4). The last observation could be expected since the depletion of the cementing species results in the reduction in the rates of metal nucleation and growth. The metal produced in the second period is likely to be less compact and more prone to fall than that in the first period, as indicated by the above different values for m_c. In addition, the critical weight m_c depends on the system investigated, being at 1.20 kg m^{-2} Ag for the 10 mol m^{-3} Ag(I) solution and only 0.24 kg m^{-2} Cd for the 4.45 mol m^{-3} Cd(II) solution.

3.2.2. *Surface observations and role of the deposit morphology*

A change in the deposit morphology was observed for the two systems, from dendrites to facets near the

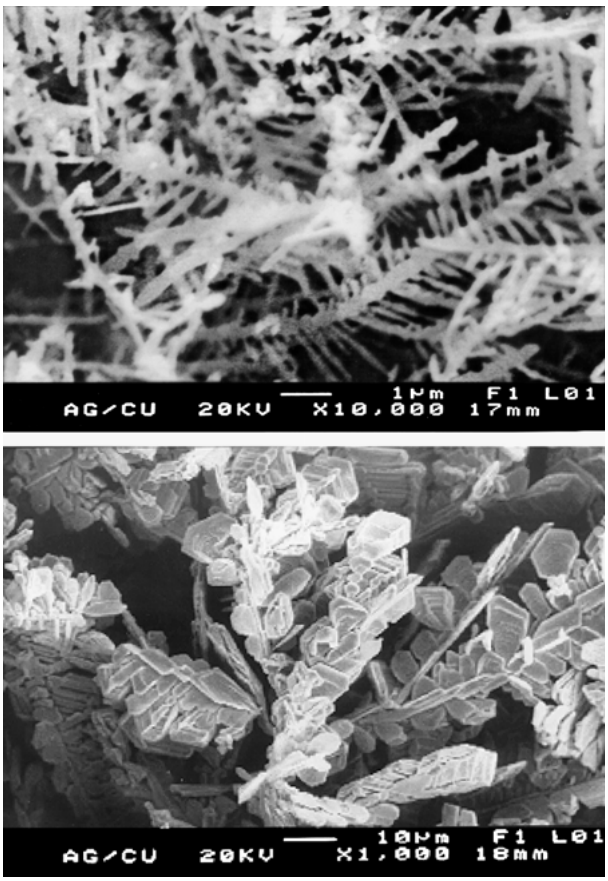

Fig. 4. Deposit morphology before (up) and after (down) the critical point for silver cementation; $\omega = 157$ rad s^{-1}, $C_0 = 10$ mol m^{-3}, $A = 0.196$ cm^2, $V_0 = 100$ cm^3.

critical point as shown in Figure 4 for the example of Ag(I)/Zn. In spite of their similar aspect, the deposits produced by the two reactions differ largely in their compactness and adherence, the silver deposit being much more brittle. Moreover, former experimental work on cadmium cementation [30] showed that the deposit morphology – and thus the critical time and enhancement factor – depended also on the experimental conditions. For instance, for initial Cd(II) concentrations over 8 mol m^{-3} the dendrites produced in the first part of the reaction turn to a globular, compact deposit during the run and the overall reaction rate was reduced. This reduction may be attributed to hindered transfer of the zinc cations produced through the cadmium deposit.

Therefore, the mass and the morphology of the depositing surface can be correlated to the cementation rate, and be discussed as a whole in terms of critical roughness: this roughness may induce a change in the flow regime near the reacting surface and enhance mass transfer rates. This is accompanied by an enhancement in the reaction rate and a change in the deposit morphology during the run.

3.3. *Corrosion*

Corrosion experiments were performed for Ce(IV)/Zn and Cr(VI)/Zn systems for investigation of the critical roughness. The rotation speed was varied from 150 to about 320 rad s^{-1} and the electrode diameter was either 5 or 9 mm.

The time variations of the concentration of Cr(VI) or Ce(IV) were plotted following Relation (3). As for cementation, the variations exhibited two linear sections with constant K_2 greater than K_1 (Figure 5), and the microcavities resulting from the anodic dissolution of the substrate may be considered to act in the same way as the formed deposit. The first period corresponds to low amounts of dissolved metal and the modification of the surface may be assumed to be limited. In contrast, the active area of the electrode is very different from the geometrical area at the end of the run. The transition between the two periods is generally less distinct than for cementation, especially with Cr(VI). The experimental error in determination of the critical point was estimated at about 20% by replicate experiments. Transition occurred at conversion extents of the corrosive agent ranging from 5 to 9% for Ce(IV) and from 7 to 15% for Cr(VI). The corresponding loss of zinc m_c was calculated for all runs from the conversion extent and taking into account the reaction stoichiometry: m_c varied from 0.08 to 0.15 kg m^{-2} with Ce(IV) and from 0.35 to 0.70 kg m^{-2} using Cr(VI).

For all tests, the electrode surface was observed at the transition time t_c by SEM. The average depth of the cavities at t_c, r_c, was determined using the optical microscope as follows. Focusing was first done on the metal surface around the cavity, and later in the cavity bottom: the difference in the heights, measured with the micrometric screw, gave estimates of the cavity depth. The accuracy in the measurements, made with 10–20 cavities per experiments, was estimated at 20%. Depth of the microcavities varied from 20 to 60 μm with Ce(IV) and from 32 to 80 μm with Cr(VI) (Table 2): higher values were observed with the larger disc electrode. This

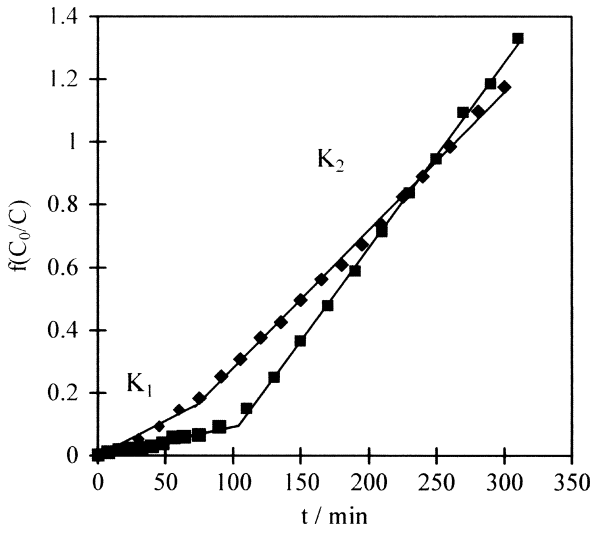

Fig. 5. Kinetic curves for corrosion reactions without deposition, with Ce(IV)/Zn (■) and for Cr(VI)/Zn (♦), both in a sulfate medium; $\omega = 157$ rad s^{-1}, $C_0 = 10$ mol m^{-3}, $A = 0.636$ cm^2, $V_0 = 325$ cm^3.

Table 2. Results of zinc corrosion experiments with Ce(IV) and Cr(VI) species at 25 °C. Comparison of dimensions r_c and l_c at the critical point with the thickness of the diffusion layer, and values of the local Reynolds number, Re_{surf}

Corrosion agent	Disc diameter /mm	Rotation rate /rpm	Roughness, r_c /μm	Thickness of the diffusion layer, δ /μm	Thickness of the dissolved layer, l_c /μm	Re_{surf}
Ce(IV)	5	1500	29	9.6	13	1.5
Ce(IV)	5	2000	25	9.0	12.8	1.7
Ce(IV)	5	2500	20	8.2	11.5	1.6
Ce(IV)	5	3000	20	4.8	11.9	2.0
Ce(IV)	9	1500	60	7.7	14.8	7.6
Ce(IV)	9	2000	60	7.0	16.2	10.3
Ce(IV)	9	3000	52	4.5	20.4	13.5
Cr(VI)	5	1500	38	11.5	63.2	2.3
Cr(VI)	5	2500	32	9.1	50	3.4
Cr(VI)	9	1500	80	7.6	64.9	10.2
Cr(VI)	9	3000	70	4.1	98.8	15.5

dimension can be compared with the thickness of the diffusion–convection layer δ, estimated from mass transfer coefficient k_1 related to the first period and the diffusion coefficient of the corrosion agent: r_c was significantly larger than δ as shown in Table 2. Additional observations of the zinc surface were also made at various times for a couple of experiments: visual analysis of the surface photograph showed the progressive change in surface morphology, with progressive increase in the mean depth with time. In the first period (i.e., before t_c) corrosion results in the formation of hexagonal cavities (Figure 6), following the crystalline lattice of zinc. In contrast, for times larger than t_c, the etched cavities are far less regular, with the formation of galleries (Figure 6): corrosion does not occur inside a grain of metal but seems to be caused by the presence of defects in the metal structure.

The nature of the corrosive solution was shown to have a significant effect on zinc corrosion. First, for the same rotation rate of the disc with identical diameter, t_c was usually shorter using Cr(VI) solutions than with Ce(IV). This could be expected from the values of rate constant K_1 which were far higher with Cr(VI) than with Ce(IV). In addition, as expressed above, Cr(VI) allowed much higher amounts of dissolved metals at t_c and formation of noticeably larger cavities. The average thickness of the compact layer of dissolved zinc l_c at time t_c, calculated from m_c and the zinc density at 7140 kg m^{-3}, varied from 11 to 21 μm with Ce(IV) and 50 to 100 μm using Cr(VI). Corrosion phenomena of zinc are of stronger intensity with Cr(VI), as estimated by comparison of dimensions l_c and r_c: with Ce(IV), l_c represents 42% within 18% of the cavity depth; in contrast, l_c can exceed r_c for the case of Cr(VI) (Table 2).

The above observations suggest the occurrence of local change in hydrodynamics in the vicinity of the metal surface, linked to an increase in surface roughness acting as a turbulence promoter. The effect of the surface roughness is discussed for corrosion only because the conversion of the oxidising species could be followed without the occurrence of side phenomena such as the fall of the deposited metal at regular intervals.

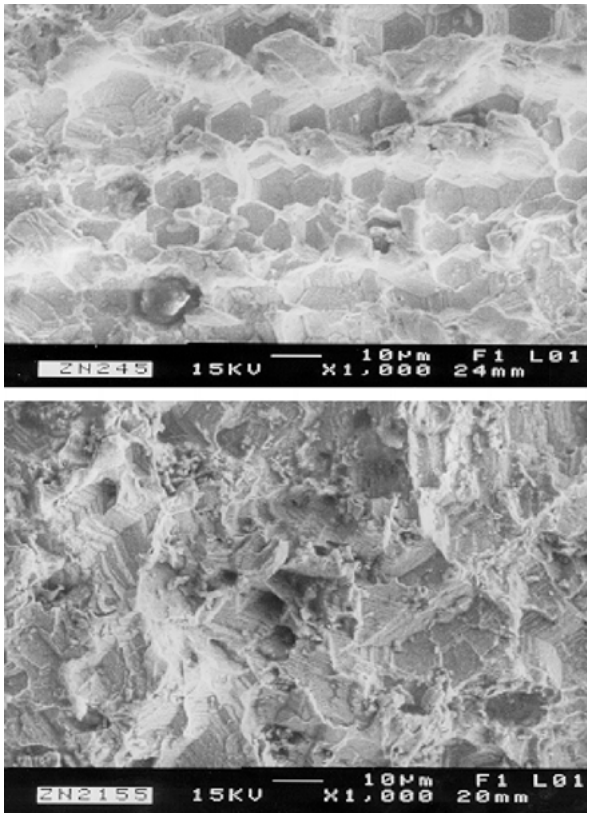

Fig. 6. Zinc surface submitted to corrosion with Cr(VI) before (up) and after (down) the critical point; $\omega = 157$ rad s^{-1}, $C_0 = 10$ mol m^{-3}, $A = 0.196$ cm^2, $V_0 = 100$ cm^3.

4. Discussion

The interpretation of the variations of $f(C_0/C)$ with time showed than mass transfer coefficients k_2 calculated over the geometrical area, varied with the rotational speed to a power in the range 1–1.4. The moderate value of the Reynolds number Re, defined as ($\omega\ r^2/\nu$), below 7000, suggested that such variation was not due to fully turbulent flow, and closer investigations of transfer phenomena appeared necessary.

4.1. *Literature survey*

The Levich expression (Relation 4) holds for laminar flow around a smooth RDE for Re below 2×10^5 [31]. Over this Re limit, mass transfer rate at the smooth surface varies with the rotation rate to the power 0.9 [32], even though transitional flow was shown to occur in the Re range $(2–8) \times 10^5$ [33, 34].

The effect of the surface roughness on the hydrodynamic regime near a RDE was previously investigated [35, 36]. Varying the Reynolds number of the 12.7 cm disc up to 5.5×10^5, Cornet et al. [35] observed the transition in flow regime by a change in the slope in the dimensionless mass transfer correlation. Their experimental values for the transition Reynolds number, Re_t, were shown to decrease with the surface roughness, k_s, in accordance with Dorfman's relation [37]:

$$Re_t = 1500\left(\frac{r}{k_s}\right)^{0.574} \tag{5}$$

Relation 5 expresses the fact that the surface irregularities act as local turbulence promoters and induce flow disruption. Experimental Re_t data varied from 2.8×10^4 to 6.5×10^4, and for k_s between 7.5×10^{-4} and 5.3×10^{-5} m. The Re_t values are significantly below the transition Re for smooth surfaces given above. Application of Relation 5 to the present case yielded Re_t values in the range $(1.5–2.4) \times 10^4$, which are from 3 to 20 times larger than the Re values of the zinc disc electrode, and such a hydrodynamic change in the corrosion experiments seems unlikely. However, Relation 5 may not hold for the case of quite small discs, with different rotation rates and roughness. In addition, the occurrence of surface change was not considered by the authors since oxygen reduction was the electrode reaction.

Besides, for cementation reactions from Cd and Cu solutions at 0.1 mol m^{-3}, coefficient k_2 measured at a 5 cm RDE was observed to vary with $Re^{0.74}$ above 1.5×10^4 [38]. The transition was observed for m_c of about 10^{-3} kg m^{-2}, and average deposit thickness below 0.1 μm, which are two orders of magnitude below the present data obtained with more concentrated solutions. Because of the different conditions, the enhanced-rate period evidenced in [38] has a physical meaning different from that shown in Figures 2, 3 and 5.

The change in electrode area and the possible disruption of the flow by the surface irregularities are discussed below. For diffusion-controlled operations, the actual electrode area corresponds to the area concerned by diffusion-convection phenomena. For asperity values below the thickness of the diffusion layer δ, transfer phenomena are not affected by the roughness of the surface and the active area can be approximated by the geometrical area. In contrast, in case that the asperity is far larger than δ, the area concerned by diffusion phenomena may exceed the geometrical area. For the case of linear patterns grooved in a flat electrode, the flow was shown formerly to be disrupted for pattern depths as low as 20 μm, depending on the aspect ratio of the cavity [39–41]. Mass transfer rate profiles exhibit sharp peaks at the edges of the cavity resulting from local flow disruption.

In the present case the hydrodynamic regime is not fully turbulent because of the moderate dimensions of the surface irregularities, but is disrupted at regular intervals. Mass transfer relationships established for smooth surfaces (e.g., Levich's relation) may be no longer valid.

4.2. *Estimation of the change in electrode area*

Mass transfer coefficients k_1 were compared to the values predicted by the Levich equation (Relation 4). The disc surface was assumed to be entirely active and the values of physicochemical parameters given in Table 1 were used. As shown in Figure 7(a), mass transfer rates obey the Levich equation for Re below 2000. For $Re > 3000$ appreciable deviation from the theoretical law occurs, in particular for the case of Cr(VI) species, with ratio (k_1/k_{Levich}) up to 2. Deviation from Levich's equation is more significant in the second period (Figure 7(b)) and ratio (k_2/k_{Levich}) was shown to

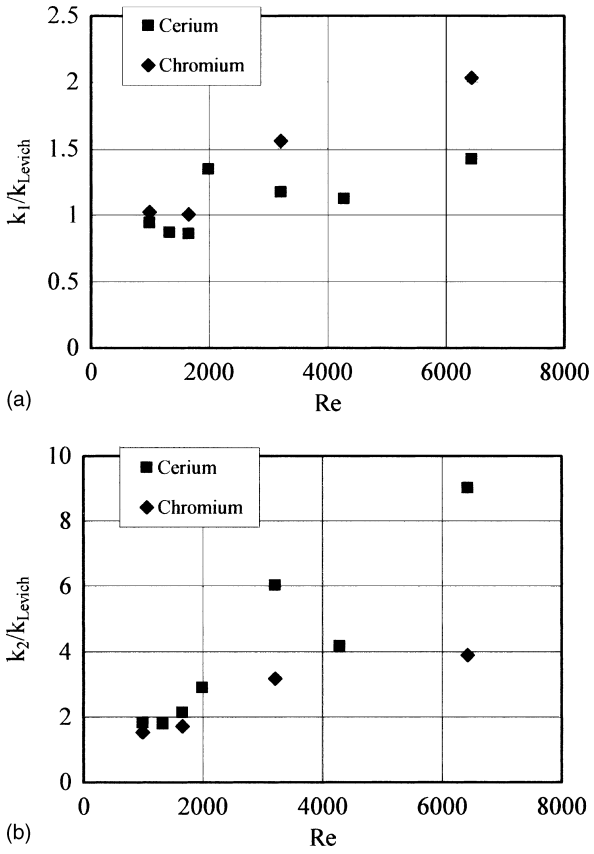

Fig. 7. Mass transfer coefficient of the electroactive species used for corrosion of zinc surface, related to the theoretical coefficient predicted by the Levich's equation: (a) first period of the corrosion run and (b) second period of the run.

increase regularly with *Re*, depending on the electroactive species. Whereas the ratio increases up to 9 for Ce(IV) at a *Re* of approximately 6500, the ratio is only at 4 for Ce(IV) at the same Reynolds number.

The change in electrode area was modelled as follows: in the first period, the cavities etched are small enough to allow the modification to be neglected, and the electrode area was assumed to correspond to the geometrical area. Beyond the transition time, the change in active area was expressed by the ratio (k_1/k_{Levich}), even though more significant changes might be expected during the second period. The mass transfer coefficient k_2 was then corrected for the surface change by Relation 6:

$$k_{2,\text{mod}} = k_2 \left(\frac{k_1}{k_{\text{Levich}}} \right)^{-1} \tag{6}$$

4.3. *Mass transfer correlations*

The experimental data were first correlated on the basis of the disc radius, as $Sh\ Sc^{-1/3}$ against *Re* (Figure 8). For the first kinetic period the following relation was obtained within 20%:

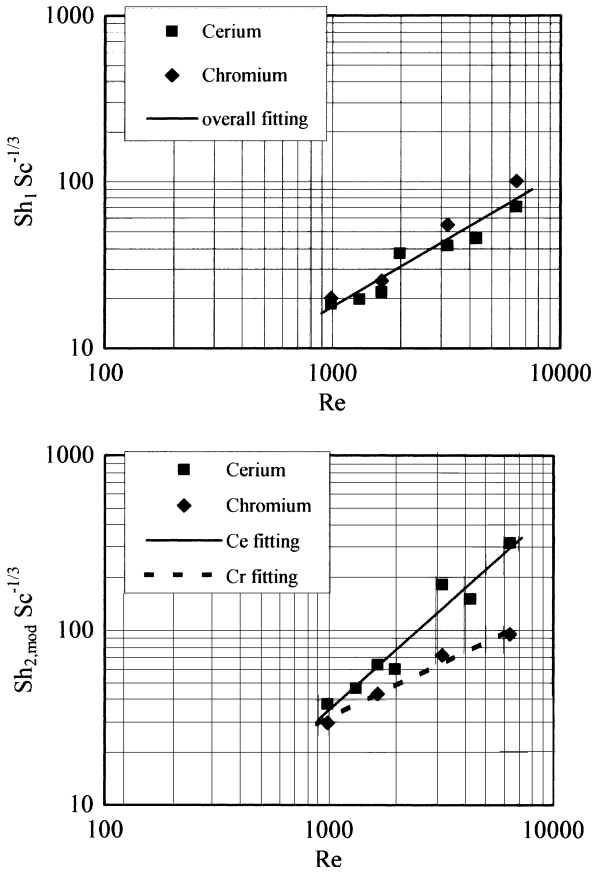

Fig. 8. Mass transfer correlations for corrosion of zinc surface, established on the disc radius; mass transfer coefficients k_2 were corrected for the change in surface after Relation 6.

$$Sh_1 = 0.068 Re^{0.8} Sc^{1/3} \tag{7}$$

with *Re* in the range 900–7000.

It can be observed that the data for Cr(VI) are noticeably above those for Ce(IV). In spite of the acceptable fitting, Relation 7 is of restricted physical meaning since the actual electrode area likely exceeds the geometrical area: this is directly linked to the deviation from Levich's equation discussed above. For the second period, the correlation depends on the nature of the etching species:

$$Sh_{2,\text{mod}} = 0.012 Re^{1.15} Sc^{1/3} \quad \text{for Ce(IV)} \tag{8a}$$

$$Sh_{2,\text{mod}} = 0.38 Re^{0.64} Sc^{1/3} \quad \text{for Cr(VI)} \tag{8b}$$

Transfer phenomena can also be discussed at local scale, considering for instance r_c as the characteristic dimension, and using the corresponding Sherwood and Reynolds numbers:

$$Sh_{\text{surf}} = \frac{k r_c}{D} \text{ and } Re_{\text{surf}} = \frac{v_{rc} r_c}{\nu} \tag{9}$$

where v_{rc} is the radial component of the velocity at distance r_c from the surface. Solution of continuity equation and Navier–Stokes equations leads to the expression of the radial velocity [42], v_z, at distance z from the surface:

$$v_z = r\omega A \tag{10}$$

where function F can be calculated by approximate functions of dimensionless coordinate ζ proportional to z. The values of F reported in Newman [43] were fitted in the ζ range 0–2 to a polynomial expression which was introduced in Equation 10. The use of this velocity in the expression of the local Reynolds was suggested in previous investigations dealing with transfer phenomena at patterned electrodes in laminar flow [41], in which the characteristic velocity was defined as the product of the wall velocity gradient to the cavity depth [40], assuming a linear velocity profile near the surface.

The experimental data were plotted using the above relations, taking into account the correction for change in active area. As for the global approach, Figure 9 shows that in the first period, mass transfer phenomena are little dependent on the nature of the oxidant. The dimensionless correlation yields an exponent value of the order of 0.73 for the two series of data. In contrast, the second part of the corrosion test is affected by the nature of the corrosion agent: $Sh_{\text{surf}}\ Sc^{-1/3}$ varies with $Re_{\text{surf}}^{0.93}$ for Ce(IV) and with $Re_{\text{surf}}^{0.62}$ for the case of Cr(VI). For both chemical systems, the local Reynolds number is in the range 1–15, depending on the disc diameter and the rotation rate (Table 2): in the vicinity of the patterns formed by the corrosion, the liquid flow possesses

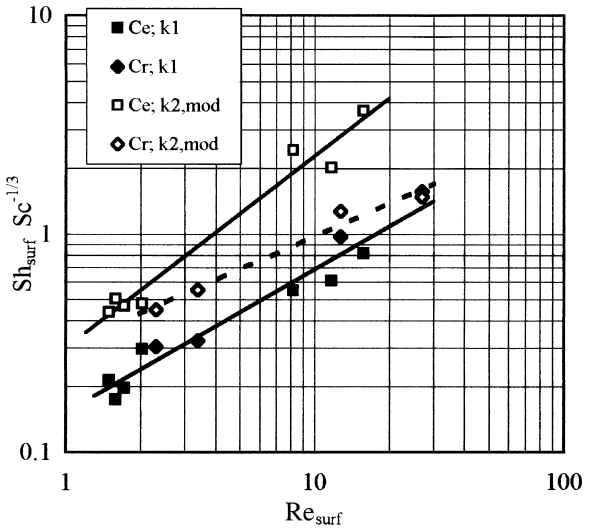

Fig. 9. Mass transfer correlations for corrosion of zinc surface, established at the local scale of the corroded surface; Mass transfer coefficients k_2 were corrected for the change in surface after Relation 6.

significant inertia which is to affect flow recirculation and mass transfer rate in the cavities.

5. Conclusions

For concentrations of the active species of the order of 10 mol m^{-3}, the transition in reaction kinetics was observed for critical weights in the range 0.1–0.7 kg m^{-2}, corresponding to the thickness of deposited/corroded layer varying from 10 to 100 μm. Experimental data revealed that the rate enhancement is due to the increase in electrode area, together with a change in flow regime induced by the irregularities of the surface submitted to deposition/corrosion. The exponents in the mass transfer correlations deduced from the experimental data, are not significantly dependent on the characteristic dimension chosen. In spite of the limited number of data, the rate of Zn corrosion caused by the action of Cr(VI) species differs largely from that with Ce(IV).

The mass transfer coefficient k_1 from corrosion with Ce(IV) are in acceptable agreement with the Levich equation, due to the moderate dimensions of the cavities formed. The deviation is larger for the case of Cr(VI) species, due to more rapid surface changes. Nevertheless, both series of data were fitted by the same mass transfer correlation, and the exponent of approx. 0.8, expresses the increase in the surface offered to diffusion–convection.

For Cr(VI), the moderate value of the mass transfer exponent in the second period suggests that the flow is disrupted by the cavities formed, with a moderate change in active area during the second period. A quite larger exponent was obtained for Ce(IV): this exponent does not correspond to any particular flow as explained below. The strong deviation from the Levich equation by factors up to 9, results from the continuous change in electrode area throughout the run, and the apparent constancy of the overall kinetic constant, K_2, may be due to partial deactivation of the electrode surface.

References

1. M.E. Wadsworth and J.D. Miller, Hydrometallurgical processes, in 'Rate Processes of Extractive Metallurgy' (Plenum Press, New York, 1979), pp. 33–244.
2. J.D. Miller, R.Y. Wan and J.R. Parga, *Hydrometallurgy* **24** (1990) 373.
3. R. Gana, M. Figueroa, L. Kattan, D. Grandoso and M.A. Esteso, *J. Appl. Electrochem.* **29** (1999) 1475.
4. D. Stanojevic, B. Nikolic and M. Todorovic, *Hydrometallurgy* **54** (2000) 151.
5. S. Hirsch and C. Rosenstein, *Metal Finish.*, (*63rd Guidebook and Directory Issue*), **93(1A)** (1995) 415.
6. T. Stefanowicz, M. Osinska and S. Napieralska-Zagozda, *Hydrometallurgy* **47** (1997) 69.
7. F. De Blander and R. Winand, *Electrochim. Acta* **20** (1975) 839.
8. K. Stole-Hansen, D.A. Wregget, D. Gowanlock and P.E. Thwaites, *Comput. Chem. Eng.* **21** (1997) S1099.
9. M.T.A. Reis and J.M.R. Carvalho, *Minerals Eng.* **7**(10) (1994) 1301.
10. P.E. Charpentier, PhD thesis, *INPG*, Grenoble, France (1997).
11. S.A. Nosier and S.A. Sallam, *Separat. Purif. Technol.* **18** (2000) 93.
12. G.P. Power and I.M. Ritchie, Metal displacement reactions, *in* B.E. Conway and J.O. Bockris (Eds), 'Modern Aspects of Electrochemistry' No. 11 (Plenum Press, New York, 1975), chapter 5, pp. 199–250.
13. G.P. Power and I.M. Ritchie, *Aust. J. Chem.* **29** (1976) 699.
14. J.D. Miller and L.W. Beckstead, *Metall. Trans. TMS/AIME* **4** (1973) 1967.
15. F. Lawson, Cementation kinetics, *in* M. Mohan Rao, K.P. Abraham, G.N.K. Iyengar and R.M. Mallya (Eds) 'Thermodynamics and Kinetics of Metallurgical Processes (ICMS-81)', (The Indian Institute of Metals, Calcutta 1985), pp. 207–225.
16. T. Angelidis, K. Fytianos and G. Vasilikiotis, *Resources, Conserv. Recycling* **2** (1989) 131.
17. G. Puvvada and T. Tran, *Hydrometallurgy* **37** (1995) 193.
18. H.H. Nguyen, T. Tran and P.L.M. Wong, *Hydrometallurgy* **46** (1997) 55.
19. V. Annamalai and J.B. Hiskey, *Trans. Soc. Min. Eng. AIME* **6** (1978) 650.
20. K. Zaghib, E. Chainet and B. Nguyen, *J. Electrochem. Soc.* **144**(11) (1997) 3772.
21. K.G. Mishra and R.K. Paramguru, *J. Electrochem. Soc.* **147**(9) (2000) 3302.
22. I.M. Ritchie and S.G. Robertson, *J. Appl. Electrochem.* **27** (1997) 59.
23. C. Alemany, J-P. Diard, B. Le Gorrec and C. Montella, *Electrochim. Acta* **41** (1996) 1483.
24. W.Y. Wei, C. Lee and H.J. Chen, *Langmuir* **10** (1994) 1980.
25. M. Pourbaix, 'Atlas d'Equilibres Electrochimiques' (Gauthier Villars et Cie, Paris, 1963).
26. S. Hassissène, PhD thesis, *INPG*, Grenoble, France (1992).
27. E.C. Lee, F. Lawson and K.N. Han, *Inst. Min. Metal.* **84** (1975) C87.
28. J.M. Nzikou, M. Aurousseau and F. Lapicque, *J. Appl. Electrochem.* **25** (1995) 967.
29. D.R. Lide, 'Handbook of Chemistry and Physics', 71st edn (CRC Press, New York, 1990–1991).
30. N.G. Pham, PhD thesis, *INPG*, Grenoble, France (1999).
31. A.J. Bard and L.R. Faulkner, 'Electrochemical Methods: Fundamentals and Applications' (J. Wiley & sons, New York, 1980).
32. V.G. Levich, 'Physicochemical Hydrodynamics' (Prentice Hall, New York, 1962).
33. D-T. Chin and M. Litt, *J. Fluid Mech.* **54**(4) (1972) 613.

34. K.K. Nigam, P. Mishra, S.N. Upadhyay, G.N. Pandey and S.D. Shukla, *Indian J. Technol.* **17** (1979) 87.
35. I. Cornet, W.N. Lewis and R. Kappesser, *Inst. Chem. Eng.* **47** (1969) T222.
36. M. Ganapathi, M.S. Krishna, G.J.V. Jagannadha Raju and C. Venkata Rao, *Indian J. Technol.* **12** (1974) 273.
37. L.A. Dorfman, 'Hydrodynamic Resistance and the Heat Loss of Rotating Solids' (Olivier & Boyd, Edinburgh, 1963).
38. E.C. Lee, F. Lawson and K.N. Han, *Hydrometallurgy* **3** (1978) 7.
39. K. Kondo, K. Fukui, K. Uno and K. Shinohara, *J. Electrochem. Soc.* **143** (1996) 1880.
40. M. Georgiadou, *J. Electrochem. Soc.* **144** (1997) 2732.
41. C. Duchanoy and F. Lapicque, *Chem. Eng. Sci.* **55** (2000) 1115.
42. W.G. Cochran, *Proc. Camb. Philo. Soc.* **30** (1934) 365.
43. J.S. Newman, 'Electrochemical Systems', 2nd edn. (Prentice Hall, Englewood Cliffs, NJ, 1991), pp. 312.